

# Seismic Detection of Solar Mesogranular-Scale Flow

M. F. Woodard

*Colorado Research Associates Division,  
NorthWest Research Associates, Inc.,  
3380 Mitchell Lane, Boulder, CO 80301-5410  
mfw@cora.nwra.com*

## ABSTRACT

Helioseismic correlation data computed from *SOHO*/MDI high-resolution Doppler images were inverted for solar flows of horizontal scale between 5 and 45 Mm. The photospheric Doppler velocity inferred from the inversions was compared with the original Doppler images at each scale. For horizontal scales greater than about 15 Mm, the seismically-inferred and directly-observed flow maps look similar, as has been seen in studies of supergranular flow. At smaller scales the similarity disappears, but regression analysis reveals significant correlation between the maps, demonstrating that solar  $p$ - and  $f$ -mode oscillations contain useful information about these flows. The slope of the computed regression plots is close to unity, indicating that mesogranular-scale flows extend at least a megameter below the photosphere.

*Subject headings:* Sun: interior; Sun: mass flows; Sun: mesogranulation; Sun: helioseismology

## 1. INTRODUCTION

The most vigorous near-surface turbulent motions in the Sun are characterized by cellular patterns with horizontal scales ranging from the one-to-two-megameter granulation scale to the roughly thirty-megameter scale of supergranulation. While granulation and supergranulation have been studied for quite some time, attention has been given to the five-to-ten-megameter *mesogranulation* scales only in the last few decades, starting with the work of November et al. (1981). Granulation has been identified as the pattern responsible for transporting the solar luminosity just below the photosphere and can be seen in intensity images. It is not clear to what extent the mesogranular- and larger-scale flows transport heat, since these flows are hard to detect in intensity measurements, but they certainly play

a role in organizing small magnetic structures and possibly in transporting fluid momentum. Early mesogranulation and supergranulation studies relied mainly on photospheric Doppler measurements and observations of the proper motions of small photospheric features such as granules and magnetic knots. In the last ten years seismic methods have become an important tool for exploring mesogranular and other flows in the solar interior. On the theoretical side, a quantitative understanding of near-surface convection and its interaction with hydrodynamic waves is emerging from detailed numerical simulations. A recent overview of surface convection is given by Nordlund et al. (2009).

As a firm theoretical framework for interpreting observations of near-surface flows has begun to emerge only fairly recently, it should perhaps not be surprising that analysis of mesogranular-scale motions has led to some controversies. There has been much discussion about whether granulation, mesogranulation, and supergranulation are distinct scales of motion, how deep the patterns go, and whether separate driving mechanisms are needed to account for them. Even the reality of mesogranulation has been debated (Rieutord et al. 2000; Muller et al. 1992; Shine et al. 2000). It was suggested early on that ionization zones might be important in driving near-surface convection (Simon & Leighton 1964; Simon & Weiss 1968), in which case the depth of the driving might be reflected in the vertical and horizontal scale of flow. Thus it might be tempting to identify mesogranular-scale flow with the first He ionization zone, at a depth of roughly seven megameters. In an alternative picture (Rast 2003), downflow plumes originating in the photosphere drive the larger scales of convection. Descending plumes of relatively cool gas, which originate in the dark lanes between photospheric granules, are seen in numerical simulations (Stein & Nordlund 2000). It is not clear, however, how deep the mesogranular flow should extend in this scenario.

Near-surface flows of twenty-to-forty-megameter horizontal scale have been probed using a number of helioseismic methods (Duvall et al. 1996; Lindsey et al. 1996; Kosovichev 1996; Duvall 1998; Duvall & Gizon 2000; Zhao & Kosovichev 2003; Braun et al. 2004; Woodard 2007; Jackiewicz et al. 2008; Hindman et al. 2009). In particular, supergranulation cells have been found to extend to depths of at least a few megameters. Seismic and other analysis has also revealed anisotropy in the surface wavevector and frequency ( $\mathbf{k} - \omega$ ) power spectrum of the supergranular velocity field (Gizon et al. 2003; Schou 2003), as well as correlation between the vertical vorticity and horizontal divergence of the field (Duvall & Gizon 2000; Gizon & Duvall 2003). The mesogranular flow regime has yet to be explored seismically. Part of the reason for this neglect may be that the signal-to-noise of seismic flow measurements degrades rapidly with decreasing horizontal scale (Gizon & Birch 2004). In spite of this difficulty, progress has been made in detecting small photospheric features (i.e., magnetic elements) with waves (Duvall et al. 2006). The fact that such features can be independently identified, in photospheric images, is crucial to their seismic detection.

This Letter describes a preliminary analysis of mesogranular-scale flow which combines measurements of the subsurface velocity, provided by helioseismic direct-modeling analysis, with independent, photospheric Doppler measurements of the flow. The present seismic analysis extends previous analysis (Woodard 2002, 2007), of supergranular-scale flow, to flows of smaller horizontal scale. The crude method, similar to that of Woodard (2002), used to invert helioseismic correlation data for subsurface flow, is outlined in Section 2 and Section 3 describes the application of the method to a datacube of high-resolution photospheric Doppler images from the Michelson Doppler Imager (MDI, Scherrer et al. 1995) on the *Solar and Heliospheric Observatory (SOHO)*. The strategy for comparing seismically-inferred and directly-observed photospheric flow maps, which addresses the problem of seismic measurement noise, is also described here, along with estimates of subsurface flow resulting from the comparison. The significance of the present findings and the prospects for improving the detection of small-scale flows are discussed briefly in Section 4.

## 2. SEISMIC DETERMINATION OF SUBSURFACE FLOW

As in a previous study of subsurface convection (Woodard 2007), I represent the flow above and beneath an observed, corotating patch of the solar photosphere in terms of a poloidal velocity field  $\mathbf{u}(\mathbf{x}, z, t)$  in a Cartesian box. Thus

$$\rho(z) \mathbf{u}(\mathbf{x}, z, t) = \sum_{\mathbf{k}\omega} (\hat{\mathbf{z}}k^2\gamma_{\mathbf{k}\omega}(z) + i\mathbf{k}\partial_z\gamma_{\mathbf{k}\omega}) \exp[i(\mathbf{k} \cdot \mathbf{x} - \omega t)], \quad (1)$$

where  $\mathbf{x} = x, y$  are horizontal coordinates such that  $x$  increases with heliographic longitude and  $y$  with heliographic latitude. The precise mapping between the  $\mathbf{x}$  coordinates and heliographic coordinates is given by Postel projection. The  $z$  coordinate is height above the  $\tau_{5000} = 1$  level of the photosphere,  $t$  is time, and  $\rho$  denotes mass density. The vertical component of the flow velocity is arbitrarily constrained to vanish at  $z = 0.496$  Mm, corresponding to the top of the Cartesian box. Accordingly, the functions  $\gamma_{\mathbf{k}\omega}$  are taken to vanish at this boundary. The above form for the flow velocity and the condition that the mass density depends only on  $z$  imply that mass is locally conserved.

The present study used correlation data in the form  $\varphi_{\mathbf{k}'\omega'}\varphi_{\mathbf{k}\omega}^*$ , where  $\varphi_{\mathbf{k}\omega}$  are weighted coefficients of the Fourier expansion of the Doppler signal  $\varphi(\mathbf{x}, t)$ . By contrast with previous direct-modeling studies, some weight is given to the oscillation signal between the ridges of oscillatory power. The direct-modeling analysis of solar flows performed to date assumes that seismic correlation data depend linearly on the flow velocity. The flow described by equation (1) is completely determined by its horizontal velocity field, whose vertical profile at  $(\mathbf{k}, \omega) = (\mathbf{q}, \sigma)$  is proportional to  $\rho^{-1}(z) \partial_z\gamma_{\mathbf{q}\sigma}$ . Therefore, the flow dependence of the data

can be written

$$E[\varphi_{(\mathbf{k}+\mathbf{q})(\omega+\sigma)} \varphi_{\mathbf{k}\omega}^*] = \int \mathcal{K}_{(\mathbf{k}+\mathbf{q})(\omega+\sigma),\mathbf{k}\omega}(z) \rho^{-1}(z) \partial_z \gamma_{\mathbf{q}\sigma} dz, \quad (2)$$

where ‘ $E$ ’ means statistical expectation. The form of the sensitivity kernel  $\mathcal{K}_{(\mathbf{k}+\mathbf{q})(\omega+\sigma),\mathbf{k}\omega}(z)$  used here is based on the forward model described in Appendix A of Woodard (2007), taking into account the different weighting of the data used for this study. The model of correlations is based on the flow-induced dynamical couplings of  $p$ - and  $f$ -mode oscillations of radial order  $n = 0 - 4$ .

For this analysis I fit seismic correlation data to a simple flow model with a depth-independent horizontal velocity. In this approximation, the vertical profiles  $\rho^{-1}(z) \partial_z \gamma_{\mathbf{q}\sigma}$  are replaced by flow parameters  $a_{\mathbf{q}\sigma}$  and the general sensitivity relation (2) simplifies to

$$\begin{aligned} E[\varphi_{(\mathbf{k}+\mathbf{q})(\omega+\sigma)} \varphi_{\mathbf{k}\omega}^*] &= \mathcal{K}_{(\mathbf{k}+\mathbf{q})(\omega+\sigma),\mathbf{k}\omega} a_{\mathbf{q}\sigma}; \\ \mathcal{K}_{(\mathbf{k}+\mathbf{q})(\omega+\sigma),\mathbf{k}\omega} &\equiv \int \mathcal{K}_{(\mathbf{k}+\mathbf{q})(\omega+\sigma),\mathbf{k}\omega}(z) dz. \end{aligned} \quad (3)$$

Least-squares estimates of the flow parameters were obtained by evaluating the expressions

$$a_{\mathbf{q}\sigma} = \sum_{\mathbf{k}\omega} \mathcal{K}_{(\mathbf{k}+\mathbf{q})(\omega+\sigma),\mathbf{k}\omega}^* \varphi_{(\mathbf{k}+\mathbf{q})(\omega+\sigma)} \varphi_{\mathbf{k}\omega}^* / \sum_{\mathbf{k}\omega} |\mathcal{K}_{(\mathbf{k}+\mathbf{q})(\omega+\sigma),\mathbf{k}\omega}^*|^2. \quad (4)$$

Like the correlation data, these estimates are also linearly sensitive to the actual depth profiles,  $\rho^{-1}(z) \partial_z \gamma_{\mathbf{q}\sigma}$ , according to

$$E[a_{\mathbf{q}\sigma}] = \int \mathcal{R}_{\mathbf{q}\sigma}(z) \rho^{-1}(z) \partial_z \gamma_{\mathbf{q}\sigma} dz, \quad (5)$$

where the form of the averaging kernel  $\mathcal{R}_{\mathbf{q}\sigma}(z)$  follows from equations (2) and (4). Examples of averaging kernels, for the mode set used in the analysis described below, are shown in Figure 1. The plotted functions resemble the  $z$  dependence of the kinetic energy density of  $f$  modes of  $1500 < \ell < 1800$  in being highly peaked near  $z = 0$ . That the flow measurement is dominated by high- $\ell$  modes should not be too surprising as the number of analyzed modes increases steadily with  $\ell$ .

### 3. ANALYSIS OF SOHO/MDI DOPPLERGRAMS

The flow velocity below and immediately above a tracked analysis region was estimated using the least-squares approach described in the previous section. The analysis used the

high-resolution *SOHO*/MDI Doppler datacube described in Woodard (2007). The sequence of images, obtained on 1999 May 31-June 1, is approximately 34 hours long and the individual images cover an approximately  $210 \times 210 \text{ Mm}^2$  corotating patch of the photosphere close to disk center. The observed Doppler signal is assumed to represent the solar velocity at height  $z = z_{\text{obs}} = 0.2 \text{ Mm}$ . The horizontal coordinates,  $\mathbf{x}$ , of the seismic model domain also serve as image coordinates. Correlation data used in this analysis were computed from Doppler signal covering the frequency and angular wavenumber ranges  $\omega/2\pi = 2441 - 5696 \mu\text{Hz}$  and  $kR_{\odot} = 412 - 1854$ .

Flow velocity fields  $\mathbf{u}(\mathbf{x}, z, t)$  were reconstructed from the seismically-determined  $a_{\mathbf{q}\sigma}$  for different ranges of  $q$  using equation (1), in which  $\gamma_{\mathbf{k}\omega}(z)$  is evaluated from the expression  $\rho^{-1}(z)\partial_z\gamma_{\mathbf{q}\sigma} = a_{\mathbf{q}\sigma}$ . The flow parameters used for the reconstructions come from a narrow frequency ( $\sigma$ ) band defined by harmonics 0 – 2 of the  $\approx 1/34 \text{ hr}$  frequency resolution of the datacube.

To facilitate comparison of the seismically-inferred and directly-observed flows, the reconstructed velocity fields at  $z = z_{\text{obs}}$  were converted to line of sight velocity  $\tilde{\varphi}(\mathbf{x}, t)$ , using the relation  $\tilde{\varphi}(\mathbf{x}, t) = \mathbf{l} \cdot \mathbf{u}(\mathbf{x}, z_{\text{obs}}, t)$ , where  $\mathbf{l}$  is the unit vector pointing from the observed photospheric patch to the observation point. The vector  $\mathbf{l}$  has  $\mathbf{x}$ - and  $t$ -dependent projections onto the heliographic horizontal and vertical unit vectors due to solar curvature and rotation.

Examples of seismically-reconstructed Doppler images are shown in Figure 2 for  $t$  close to the midpoint  $t_{\text{mid}}$  of the observations. For comparison, Figure 2 also shows  $\varphi(\mathbf{x}, t_{\text{mid}})$ , the MDI Doppler data, after filtering to match the frequency-wavenumber selectivity of the corresponding seismic reconstructions. As expected from previous seismic analyses, the seismically-reconstructed Doppler velocity matches the directly-measured velocity fairly well on supergranular scales. But the correlation clearly degrades with decreasing spatial scale.

To explore the velocity correlations more quantitatively, I plotted seismically-inferred Doppler velocity against directly-observed velocity and computed linear correlation coefficients. Figure 3 shows  $\text{Re} [\tilde{\varphi}_{\mathbf{q}\sigma}]$  versus  $\text{Re} [\varphi_{\mathbf{q}\sigma}]$  plotted over  $\text{Im} [\tilde{\varphi}_{\mathbf{q}\sigma}]$  versus  $\text{Im} [\varphi_{\mathbf{q}\sigma}]$  for each of the wavenumber ranges of Figure 2. The  $\sigma$  range covered by these plots corresponds to the zeroth and first harmonics of the inverse data duration. In order of decreasing spatial scale, the correlation coefficients between the seismic and direct samples are 0.83, 0.82, 0.60, and 0.39 with 312, 576, 1200, and 2360 samples respectively. Note that angular wavenumber  $qR_{\odot} = 500$  corresponds to a horizontal scale of approximately 8.75 Mm, so that while this study covers the *spatial* scales of mesogranulation, it fails to span the  $\sigma$  range implied by the  $\sim 2$ -hr lifetime of this convective scale.

The correlation seen in the flow maps is again readily apparent at low wavenumber. In particular, the scatter of the seismically-inferred and directly-observed samples is approximately the same at the lowest wavenumbers. The  $\ell = 100$  case is the well-studied supergranulation scale. At the highest wavenumbers, however, the scatter in the seismic samples significantly exceeds the scatter in the direct samples. Both the lack of similarity of the seismic and direct Doppler maps and unpublished analysis based on a theoretical model of the measurement noise (Gizon & Birch 2004) suggest that at large  $qR_{\odot}$  noise contributes more than actual flow variations to the measurement scatter. Despite the considerable scatter in the seismic measurements at high  $q$ , the measured correlation coefficients are highly significant for each  $q$  range analyzed.

As a further exercise in studying correlation, some binning and averaging of the raw scatter plots was performed. For each plot, the horizontal axis was divided into bins and the average of the vertical values of points whose horizontal value lay within a bin was plotted against the midpoint of the bin. The binned scatter plots are also shown in Figure 3. The binned points fall closer to straight lines, with slopes near unity. According to equation (5), the seismic measurements are weighted averages of the horizontal flow velocity at different depths, with weighting functions shown in Figure 1. (Note that these kernels strictly apply to the case of a steady flow, though the inversions were carried out for a range of  $\sigma$  near zero frequency.) A slope of one in Figure 3 is nominally the signature of a flow of the form given by equation (1), with a depth-independent horizontal velocity. Therefore, the binned scatter plots are consistent with flows whose horizontal velocity at a given horizontal scale, averaged over the roughly 1-Mm depth range of measurement sensitivity, is close to the photospheric velocity at the same scale.

#### 4. CONCLUSION AND OUTLOOK

The present work demonstrates that solar mesogranular-scale flow produces a detectable seismic signal. Although the rapid decrease in the signal-to-noise of the measurement with increasing wavenumber seems to preclude the detection of individual flow cells of  $qR_{\odot}$  exceeding roughly 400, the collective effect of motions on these scales is clearly discernible in the data. The detection method used in this work, which relies on a comparison with non-seismic measurements of the photospheric flow velocity, senses only the component of the velocity field which correlates with the photospheric field. The numerical simulations of convection performed by Benson et al. (2006) show granular-, mesogranular-, and supergranular-scale patterns extending well below the photosphere. A regression analysis of the velocity field from these simulations (Figure 2 of Braun *et al.* 2007) quantitatively confirms that the

photospheric flow, over a range of scales including mesogranulation, penetrates many megameters into the solar interior. The present findings about depth dependence are therefore at least roughly compatible with the picture provided by recent simulations.

It should be possible to detect flows of smaller scale and shorter lifetime than those probed here. Scattering theory in the Born approximation (e.g., Cohen-Tannoudji et al. 1977) implies a lower limit of  $\lambda/2$  on the scale that waves of wavelength  $\lambda = 2\pi/k$  can resolve. This criterion is certainly satisfied for 5 Mm ( $qR_{\odot} \approx 800$ ) scales by 3 mHz ( $kR_{\odot} \approx 800$ )  $f$  modes, which suggests that somewhat smaller scales are within reach. Achieving sub-wavelength resolution appears to be mainly a signal-to-noise issue, which can be dealt with by analyzing sufficiently large volumes of data. Similarly, the behavior of the subsurface flow velocity can in principle be explored over times as short as the inverse bandwidth ( $\sim 5$  min) of the solar oscillations.

Of course, one would like to do more than just detect flows. Inversions based on forward models of general flows (e.g., Jackiewicz et al. 2008) are expected to provide a clearer picture of the depth dependence of convection on mesogranular and smaller scales. In addition to providing constraints on the component of the subsurface flow which is correlated with surface flow, rigorous inversions should be capable of providing information about uncorrelated components. A more complete investigation of mesogranular- and smaller-scale flows will require improvements in helioseismic forward models. The inadequacies of current forward models are of greater concern for smaller-scale, more-compressible flows than they are for supergranulation. Disentangling the effects of density, sound speed, and fluid velocity associated with these flows is expected to be a challenging task. Artificially-generated oscillation data, particularly wave data from simulations of convection, are expected to play an increasingly important role in the development of these models.

I thank Aaron Birch for providing eigenfunctions and other products derived from a realistic solar model and an anonymous referee for invaluable help with the manuscript. The Solar Oscillations Investigation-Michelson Doppler Imager experiment on *SOHO* is supported by NASA contract NAG5-3077 at Stanford University. *SOHO* is a project of international cooperation between ESA and NASA. This research was supported by NASA under contract NNH07CD06C.

## REFERENCES

- Benson, D., Stein, R., & Nordlund, Å. 2006, in *Astronomical Society of the Pacific Conference Series*, Vol. 354, *Solar MHD Theory and Observations: A High Spatial Resolution Perspective*, ed. J. Leibacher, R. F. Stein, & H. Uitenbroek, 92
- Braun, D. C., Birch, A. C., & Lindsey, C. 2004, in *ESA Special Publication*, Vol. 559, *SOHO 14 Helio- and Asteroseismology: Towards a Golden Future*, ed. D. Danesy, 337
- Cohen-Tannoudji, C., Diu, B., & Laloë, F. 1977, *Quantum Mechanics* (John Wiley & Sons)
- Duvall, T. L., D’Silva, S., Jefferies, S. M., Harvey, J. W., & Schou, J. 1996, *Nature*, 379, 235
- Duvall, Jr., T. L. 1998, in *ESA Special Publication*, Vol. 418, *Structure and Dynamics of the Interior of the Sun and Sun-like Stars*, ed. S. Korzennik, 581
- Duvall, Jr., T. L., Birch, A. C., & Gizon, L. 2006, *ApJ*, 646, 553
- Duvall, Jr., T. L. & Gizon, L. 2000, *Sol. Phys.*, 192, 177
- Gizon, L. & Birch, A. C. 2004, *ApJ*, 614, 472
- Gizon, L., Duvall, T. L., & Schou, J. 2003, *Nature*, 421, 43
- Gizon, L. & Duvall, Jr., T. L. 2003, in *ESA Special Publication*, Vol. 517, *GONG 2002. Local and Global Helioseismology: the Present and Future*, ed. H. Sawaya-Lacoste, 43–52
- Hindman, B. W., Haber, D. A., & Toomre, J. 2009, *ApJ*, 698, 1749
- Jackiewicz, J., Gizon, L., & Birch, A. C. 2008, *Sol. Phys.*, 251, 381
- Kosovichev, A. G. 1996, *Bulletin of the Astronomical Society of India*, 24, 191
- Lindsey, C., Braun, D. C., Jefferies, S. M., Woodard, M. F., Fan, Y., Gu, Y., & Redfield, S. 1996, *ApJ*, 470, 636
- Muller, R., Auffret, H., Roudier, T., Vigneau, J., Simon, G. W., Frank, Z., Shine, R. A., & Title, A. M. 1992, *Nature*, 356, 322
- Nordlund, Å., Stein, R. F., & Asplund, M. 2009, *Living Reviews in Solar Physics*, 6, 2
- November, L. J., Toomre, J., Gebbie, K. B., & Simon, G. W. 1981, *ApJ*, 245, L123
- Rast, M. P. 2003, *ApJ*, 597, 1200

- Rieutord, M., Roudier, T., Malherbe, J. M., & Rincon, F. 2000, *A&A*, 357, 1063
- Scherrer, P. H., Bogart, R. S., Bush, R. I., Hoeksema, J. T., Kosovichev, A. G., Schou, J., Rosenberg, W., Springer, L., Tarbell, T. D., Title, A., Wolfson, C. J., Zayer, I., & MDI Engineering Team. 1995, *Sol. Phys.*, 162, 129
- Schou, J. 2003, *ApJ*, 596, L259
- Shine, R. A., Simon, G. W., & Hurlburt, N. E. 2000, *Sol. Phys.*, 193, 313
- Simon, G. W. & Leighton, R. B. 1964, *ApJ*, 140, 1120
- Simon, G. W. & Weiss, N. O. 1968, *Zeitschrift fur Astrophysik*, 69, 435
- Stein, R. F. & Nordlund, Å. 2000, *Sol. Phys.*, 192, 91
- Woodard, M. F. 2002, *ApJ*, 565, 634
- . 2007, *ApJ*, 668, 1189
- Zhao, J. & Kosovichev, A. G. 2003, in *ESA Special Publication, Vol. 517, GONG 2002. Local and Global Helioseismology: the Present and Future*, ed. H. Sawaya-Lacoste, 417–420

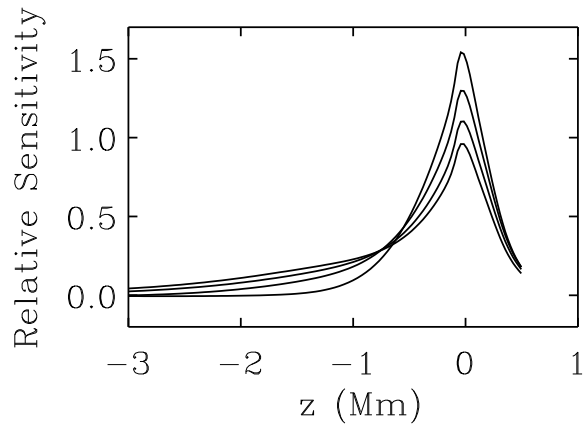


Fig. 1.— Averaging kernels  $\mathcal{R}_{q,\sigma=0}(z)$  for steady flow, as defined by equation (5), at  $qR_{\odot} = 100, 200, 400,$  and  $800$ . The sensitivity to the horizontal flow velocity becomes shallower with increasing  $q$ .

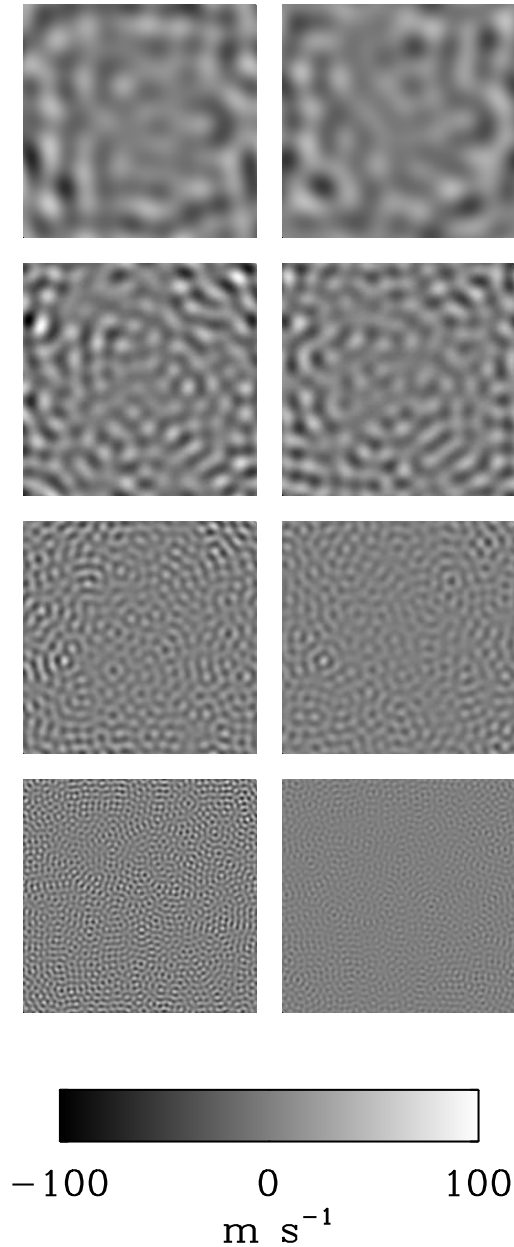


Fig. 2.— Horizontal-wavenumber- and frequency-filtered photospheric Doppler maps (blue shift), as described in the text. The left panels are seismic reconstructions ( $\tilde{\varphi}$ ) and the right panels are directly-observed maps ( $\varphi$ ). From top to bottom, the mean angular wavenumber of the filter is  $qR_{\odot} = 100, 200, 400, 800$ , with a width of 100 in each case.

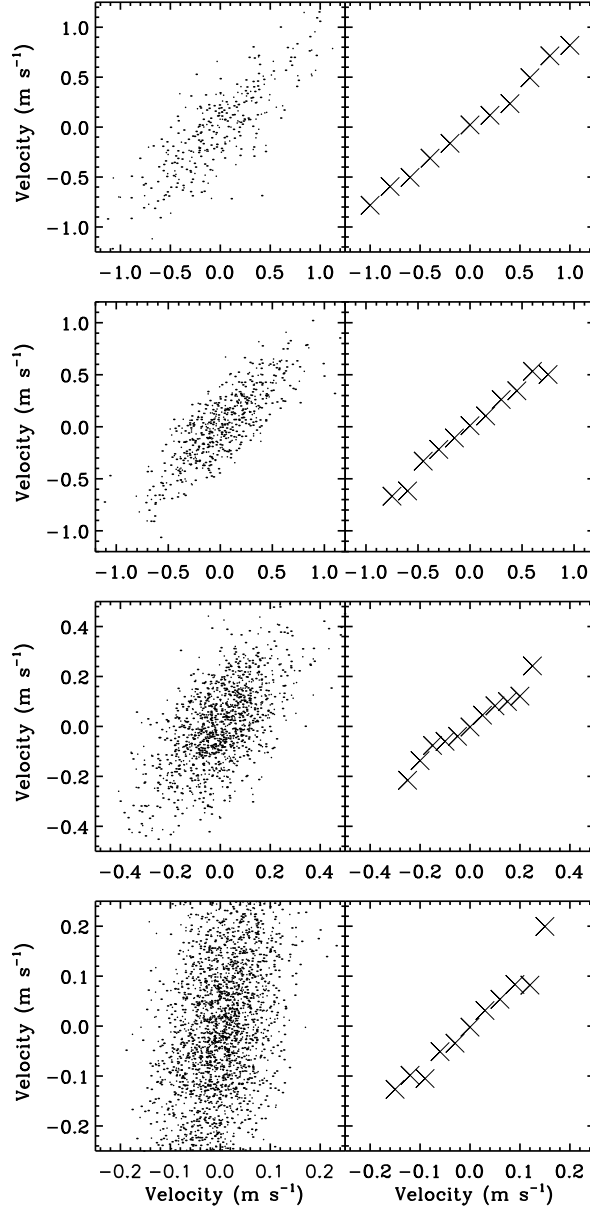


Fig. 3.— Real and imaginary parts of the Fourier coefficients of the seismically-inferred Doppler signal,  $\tilde{\varphi}$ , plotted as a function of the corresponding coefficients of the directly-observed signal,  $\varphi$ , as described in the text. Results for flows of different horizontal scale are in the vertical order of Fig. 2. The left panels show raw samples and the right panels show the corresponding binned samples.